Measurements of x rays and γ rays from stopped kaons*

Clyde E. Wiegand and Gary L. Godfrey
Lawrence Berkeley Laboratory, University of California, Berkeley, California 94720
(Received 16 January 1974)

Intensities have been measured for 346 x-ray lines of kaonic atoms of elements and pure isotopes ranging from $Z = 2$ through $Z = 92$. Within experimental accuracy, isotopes of the same elements yielded equal intensities. However, a remarkable variation in intensities versus Z was observed for kaonic transitions believed not to be significantly influenced by nuclear absorption. Fourteen x-ray lines from Σ^--hyperonic atoms of light and medium-Z elements were measured. Also observed were 29 nuclear γ-ray lines that followed kaon capture.

I. INTRODUCTION

Stopped negative mesons are captured into atomic states of large principal quantum number n. The systems are then called "mesonic atoms." After the early stages of deexcitation by Auger processes, the meson orbits the nucleus at radii smaller than that of the ground-state electrons. Deexcitation then proceeds mainly by the emission of x rays, and by their x-ray spectra these hydrogenlike systems have been studied for many years. The first observed x-ray lines were from pionic atoms in 1952[1] followed by muonic x rays in 1953.[2] Four kaonic x-ray spectra of light elements were published by Wiegand and Mack in 1967.[3] Measurements were made on the spectra of many medium and heavy elements by Wiegand in 1969.[4] In the past three years other groups of experimenters have become active in the study of kaonic x rays; namely, Backenstoss *et al.*[5] and Barnes *et al.*[6]

Muons have turned out to be excellent probes of the distribution of nuclear charge.[7] Their interaction is practically exclusively with the Coulomb field of protons and their orbits extend deep within nuclear matter. Pions, through the short-range nuclear force, interact mainly with two nucleons simultaneously. Although the study of pionic x rays is complicated by the two-nucleon requirement, it has given interesting results on the pion-nucleus interaction, especially through broadened and shifted lines.[8]

Jones and Wilkinson[9] expected kaons to be excellent probes of the nuclear surface because they react strongly with single neutrons and single protons. However, complications have been encountered that prevent simple explanations of the kaonic x-ray spectra in terms of the distribution of neutrons and protons at the nuclear surface.

The main object of the presently described experiment was to obtain and catalog the spectral lines that result from stopping negative kaons in elements ranging from $Z = 2$ through $Z = 92$. Primary interest was in the x rays resulting from transitions between the lowest Bohr orbits reached before the kaons disappeared through reactions with peripheral nucleons. Along with the kaonic x rays there appeared x rays from Σ^- hyperonic atoms and many nuclear γ rays. Tables IV, VII, and VIII are a compilation of the results.

A cursory survey of kaonic x rays can be obtained by referring to Fig. 7, a chart of the intensities of the principal ($\Delta n = -1$) transitions versus Z. For general discussions of mesonic atoms and extensive lists of references, see Burhop and Kim.[10]

II. APPARATUS

A. Beam

Negative kaons were produced in a target of tungsten in the external proton beam of the Bevatron. The size of the target was 0.762 cm wide by 0.508 cm high by 5.08 cm along the beam. The energy of the proton beam was approximately 5.6 GeV. Its intensity averaged about 5×10^{11} protons per machine burst and the duration of each burst was about 1 sec, repeated every 6 sec. Although the beam contained some temporal fine structure, the experiment was unaffected because all instantaneous counting rates were comfortably within the capability of the apparatus. The beam was focused on the target into a spot whose mean diameter was estimated to be 0.2 cm. Kaons and other particles produced in the forward direction entered a mass spectrometer whose first elements were a quadrupole lens Q_1 and a bending magnet M_1 as indicated on the beam plan of Fig. 1.

The quadrupoles Q_2 and Q_3 focused the beam onto a combined momentum and mass slit near the end of the electrostatic separator whose electric field was vertical and compensating magnetic field was horizontal. The slit opening was 1 cm high by 7 cm wide formed by blocks of uranium 20.32 cm

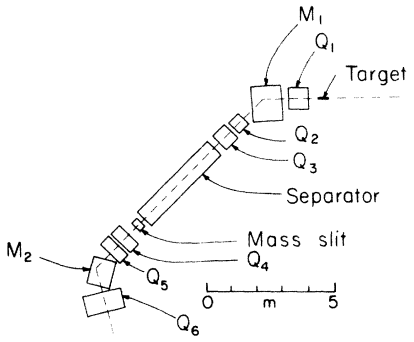

FIG. 1. Plan of kaon beam showing arrangement of quadrupoles Q, bending magnets M, and electrostatic separator.

thick. Particles of momentum 500 MeV/c were steered to the vertical center line of the slit by bending magnet M_1. The vertical electric field and the horizontal magnetic field deflected kaons through the horizontal "mass" slit. Particles lighter than kaons were deflected above the mass slit. Quadrupoles Q_4, Q_5, bending magnet M_2, and quadrupole Q_6 constituted the second leg of the mass spectrometer.

B. Kaon counters

Kaons were identified by a series of counters beginning with scintillator S_1, placed directly behind the mass slit. A group of counters consisting of water Cerenkov C_1, scintillators S_2, S_3, S_4, and S_5 were located as shown in Fig. 2. The electrostatic separator did not remove all the pions from the second leg of the spectrometer. Identification of kaons in the presence of the background of pions was accomplished by connecting the water Cerenkov counter in anticoincidence to the main set of counters and by making use of the difference in the time of flight of pions and kaons between counters S_1 and S_2. The distance between S_1 and S_2 was 5.2 m. At 500 MeV/c the difference in time of flight between kaons and pions was 6.3 nsec. Counter S_5 was connected in anticoincidence and further reduced the chance of mistaking a beam pion for a kaon because the probability was negligible that beam pions of 280 MeV would stop in the targets. S_5 was placed downstream from the targets to reduce the probability that charged products resulting from kaon reactions would strike the counter and veto legitimate stopped kaon signals. A curve showing the separation of kaons from pions as a function of separator magnet current appears in Fig. 3. Table I lists the principal beam parameters.

Beam kaons were additionally identified by their range in the energy degrader which was, for 500 MeV/c, 47 g cm^{-2} carbon. The thickness of the graphite degrader was adjusted to maximize the number of kaons stopped in the targets. This was done experimentally and a range curve is shown in Fig. 4. The measured range checked with expected range of 500 MeV/c kaons.

C. Targets

All except two special targets (He and LiH) were 8.9-cm diameter and were mounted on a wheel in a standard geometry as indicated in Fig. 2. Target thicknesses were 2 g cm^{-2} thick (2.8 g cm^{-2} along the beam line) except in a few instances where there was not enough material available to make the standard thickness. Powdered and liquid materials were contained within pill-box-shaped vessels made from stock methyl-methacrylate tubing 10.16-cm outside diameter (8.9-cm inside diameter). The flat sides of the containers were of Mylar of appropriate thickness, usually ≤ 0.0127 cm thick. Metal foil targets were fixed within standard sized plastic rings.

Many of our targets were greater than 99%-pure isotopes or chemical compounds of pure isotopes obtained from the Cross-Section pool of the Oakridge National Laboratory. All the isotopic targets were contained in our standard boxes filled at the Isotopes Development Center at Oakridge.

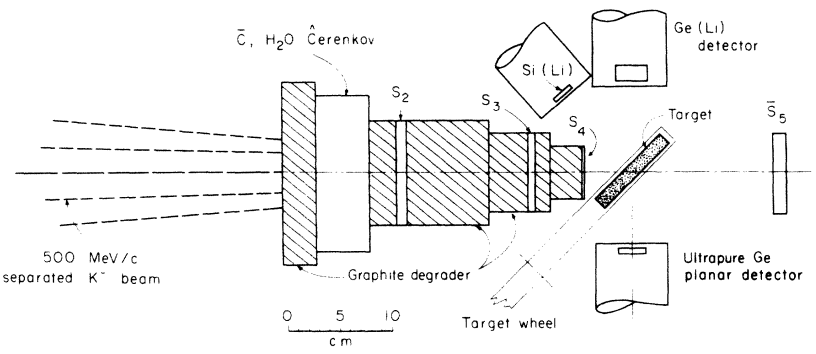

FIG. 2. Diagram of the arrangement of the beam counters, target wheel, and semiconductor detectors. The targets were approximately 65 cm from the exit of quadrupole Q_6.

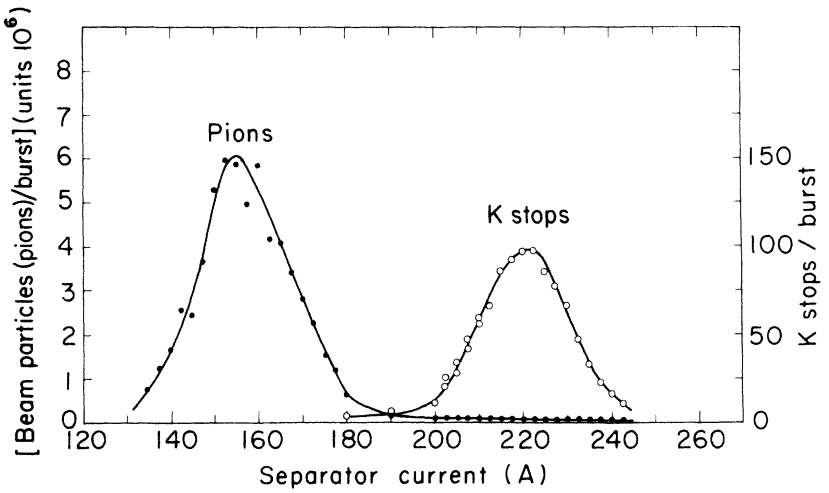

FIG. 3. Plots of beam pions and stopped kaons vs separator magnet current. Note different scales for pions (left) and kaons (right-hand side). The separator's magnetic field compensated for the electrostatic deflection and allowed particles of preferred velocity to pass through the slits of the spectrometer.

We are grateful for their cooperation.

There was only one known case where target impurities made trouble. A target made from "off-the-shelf" natural lithium was found to be contaminated, mainly with copper. There was enough copper in the target to show two prominent Cu fluorescent x-ray lines and to attenuate the soft kaonic x rays. A target of ^{6}Li handled in the same way as the natural Li target was uncontaminated.

The LiH target was about 6×10 cm^2 by 1.9 g cm^{-2} thick. It was not mounted on the target wheel.

Liquid ^{4}He at 2.5°K was the other special target.[11] It was contained in a flask 10 cm in diameter by 10 cm high. The liquid was condensed from a closed system by means of a heat exchanger. Access to the He was through a window 7.6 cm high that encompassed the flask like a belt around its midsection. Kaons entered the target and x rays emerged through the window which consisted of Mylar of total thickness 0.06 g cm^{-2}.

D. x-Ray spectrometers

X rays were detected by three varieties of semiconductor devices: lithium-drifted silicon, Si(Li); lithium drifted germanium, Ge(Li); and ultrapure germanium, Ge. The detectors and their associated electronic equipment were furnished by the Lawrence Berkeley Laboratory (LBL) Nuclear Instrumentation and Electronic Engineering Groups. They were the latest in a series of spectrometers developed by Hansen, Landis, Goulding, and Jaklevic.[12]

At this point we discuss briefly the ultimate resolution of Ge and Ge(Li) detectors as it is presently known. If there were no noise in the system, the resolution full width at half-maximum (FWHM) would depend only on statistics:

$$\Delta E\ (\mathrm{FWHM}) = 2.36(E\epsilon F)^{1/2},$$

where E is the energy deposited in the detector, ϵ is the average energy to make an electron-hole pair (2.94 eV for Ge), and F is the Fano factor defined as the mean-square fluctuation divided by the average number of ion pairs. In the best detectors thus far made, $F = 0.08$.[13] Noise resolutions of 150-eV FWHM are readily achieved by well-designed systems. The observed x-ray resolution is assumed to be

$$\Delta E\ (\mathrm{FWHM}) = [P^2 + (2.36)^2 E\epsilon F]^{1/2},$$

where P is the random noise determined, for

TABLE I. Beam parameters.

Proton energy	5.6 GeV
Proton intensity	averaged 5×10^{11}/ burst
Beam bursts	1-sec duration at 6-sec intervals
Target: tungsten	$0.762\times0.508\times5.08$ cm^3
Particle momentum	500 MeV/c
Separator: electrostatic	560 KV/10 cm, 3 m long
Slit	1 cm (mass) × 7 cm (momentum)
Length of beam	14 m
Negative pions per burst through counter S4	$\sim10^5$
Negative kaons per burst stopped in 2.8 g cm^{-2}	~100

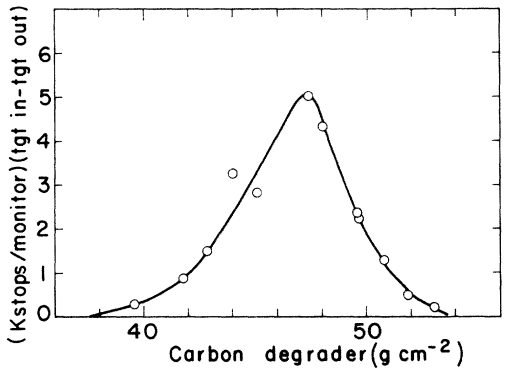

FIG. 4. Plot of stopped kaons vs thickness of graphite degrader. Beam momentum was 500 MeV/c. Target thickness was 2.8 g cm^{-2} in the direction of the beam.

example, by the width of lines made by a pulse generator. (This is actually the method used to measure F as explained in Ref. 12.) Under the assumptions that $F=0.08$, $\epsilon=2.94$ eV, and $P=150$ eV, the resolution at 100 keV would be 400-eV FWHM. Noise fluctuations and statistical fluctuations would be equal at 17 keV and amount to 220 eV.

The ultrapure Ge detector was constructed with a built-in guard ring.[14] Its effective diameter was 1.8 cm and its thickness 0.4 cm. A pulsed-light feedback scheme was incorporated into the amplifier system.[12] The outstanding performance of this detector is illustrated by the kaonic x-ray spectrum of CCl_4 in Fig. 6. At 85 keV the peak-to-background ratio was 29 and the resolution was 580-eV FWHM under actual operating conditions.

The Si(Li) detectors were 1.8 cm in diameter by 0.4 cm thick. Their amplifiers also used the pulsed-light feedback system. Resolution of the Si(Li) detectors was 340 eV at 7 keV as illustrated by the kaonic x-ray spectrum of He (see Fig. 13). Table II lists some characteristics of the principal detectors.

Signals in the main amplifiers were shaped and passed through linear gates and thence via a multiplexer to a common pulse height to digital converter of 4096 channels. In another section of the amplifiers, detector signals containing timing information were processed by logic circuits called pile-up rejectors. The function of the pile-up rejectors was to discard pulses whose temporal spacing was insufficient to avoid interference in their pulse-height measurements. Pulses that passed the noninterference test, and were in coincidence with kaon stop signals, opened the linear gates to allow the shaped pulses to enter the digitizer and subsequent data-storage registers. Timing between kaon stop and detector output signals was not stringent; 1 μsec was a typical resolving time. The interval to make a single pulse-height measurement varied from 2 to 17 μsec. These intervals were mainly occupied by the amplifier pulse lengths; the longer measurement intervals gave better energy resolution.

TABLE II. List of semiconductor detectors used in this experiment.

Designation	Material	Volume (cm^3)	Thickness (cm)	Operating bias V
D-20	Si(Li)	1.0	0.4	−320
553	Si(Li)	1.0	0.4	−375
58A	Ge(Li)	8.2	0.95	−1600
102-4	Ge(Li)	8.2	0.95	−1600
239A	Ge(Li)	13.5	1.2	−1800
148	Ge	1.0	0.4	−400

For any detector signal in coincidence with a kaon stop, all amplifier pulse-height outputs were converted to digital numbers from 0 to 4096. The pulse-height information along with a serial number and a run number were held temporarily in a storage unit. When an appropriate number of events had been stored, the core storage output was written on magnetic tape. Core readout occurred between Bevatron beam spills. The time needed to digitize and register an event was about 250 μsec. Beam spills averaged about 1 sec in duration and during these intervals three to ten events were usually recorded. Therefore, the dead time of the spectrometer was insignificant.

Data on the tapes were processed at the LBL computer center. Recording each event separately made the data processing more flexible than if an ordinary pulse-height analyzer had been used in which pulses recorded in the same bin lose their identity. For example, two or more adjacent channels of the digital converter could be summed to make spectra of less detail but with better statistics. In other words, we could increase the energy per bin in order to more nearly match the particular detector resolution. Also, the data could easily be processed in sections to check for internal consistencies.

The run numbers written on each tape record automatically included a digit that specified the target wheel position. Only tape records with identical run numbers were tabulated into a given spectrum. This procedure avoided bookkeeping errors, one of which could have vitiated an experiment designed to find differences among isotopes of the same element.

III. DETERMINATION OF STOPPED KAONS

In order to determine the kaonic x-ray intensity on an absolute basis, it is necessary to know the

number of kaons stopped in the target for each spectrum. One of the first barriers to the determination is the impossibility of placing an anticoincidence counter around or adjacent to the target because charged particles from kaon reactions with nuclei would veto many legitimate kaon stops. For this reason, S_5 was placed 18 cm from the target so that it would reject pass-through pions and kaons but would subtend only a reasonably small solid angle with respect to the target.

We define

$$K_{\text{beam}} \equiv S_1 \cdot \bar{C} \cdot S_2 \cdot S_3,$$

and

$$K_{\text{stop}}\ (\text{registered}) \equiv S_1 \cdot \bar{C} \cdot S_2 \cdot S_3 \cdot S_4 \cdot \bar{S}_5.$$

By inspection of the range curve of Fig. 4 and the geometry illustrated by Fig. 2, it is apparent that not all the kaons that fulfilled the requirements of K_{stop} (reg'd) actually stopped in the target. Some of the kaons were scattered by the degrader and missed the target entirely, and some passed through the target, but missed $\bar{S}_5$. To find the true number of kaons that stopped in the targets, K_{stop} (true), we made use of the decay properties of positive kaons. A plastic scintillation counter (composition closely equivalent to CH) of standard thickness 2 g cm^{-2} was placed in the standard target position. A scintillation-counter telescope was installed to view the target region. It consisted of two counters, T_1 and T_2, each 1 cm thick. The solid angle subtended by the telescope was determined by the front counter, T_1, which was 10.2×10.2 cm^2 at a distance of 35.5 cm from the center of the target which was then the counter, S_{target}. T_2 was 19×19 cm^2 and was situated 5 cm behind T_1.

We then reversed all magnets except that of the separator to obtain a beam of positive kaons. The constancy of the ratio, K_{stop} (reg'd)/K_{beam}, verified that the negative- and positive-beam geometries were practically the same. The target counter, S_{target}, was then put in coincidence with K_{stop}(reg'd) and a separate coincidence was formed of T_1 and T_2. A time-to-height converter and a pulse-height analyzer were used to measure muons and pions from the reactions: $K^+ \rightarrow \mu^+ + \nu$ and $K^+ \rightarrow \pi^+ + \pi^0$. The decay curve showed the kaon lifetime, 12.4 nsec. Copper absorbers were placed in front of T_1 and between T_1 and T_2 to obtain a range curve of the decay products. Using the muon component we found that $0.7K_{\text{stop}}$(reg'd) appeared to stop and decay in the target counter.

For our standard-thickness targets we used $K_{\text{stop}}(\text{true}) = 0.7K_{\text{stop}}(\text{reg'd})$. We estimated the error in the target efficiency factor (0.7) to be ±10%. The assignment of a 10% error in the number of stopped kaons is admittedly somewhat arbitrary. There is, for example, a slight uncertainty in the K-decay branching ratio that should be applied to the K^+ decay measurements because a small number of muons from $K^+ \rightarrow \mu^+ + \pi^0 + \nu$ could have been counted. There is also the possibility that some of the kaons filtered out of the target and decayed in flight within the cone of acceptance of the telescope, $T_1 \cdot T_2$. In addition, it may not be accurate to assume that the geometries of the positive and negative kaon beams were the same. Moreover there might have been other small effects that we have not considered.

It was difficult to determine the number of kaons stopped in the He, and the effective solid angle subtended by the detectors. As an aid in estimating the number of stopped kaons, we constructed an "artificial" He target (actually made of carbon dust) that had the same geometric configuration and electron density as the real He. We assumed that the same fraction of beam kaons stopped in the real He and "artificial" He and that the effective solid angle was the same in the two cases. Then the following relation applies:

$$\frac{K_s(\text{He})}{K_b(\text{He})} = \frac{K_s(\text{artificial He})}{K_b(\text{artificial He})},$$

where K_s is the true number of stopped kaons in He (or artificial He) and K_b is the number of kaons in the beam incident on the targets. The K_s (artificial He) was calculated from the intensity of the $n = 4 \rightarrow 3$ transition in C as measured in the standard geometry of the target wheel.

There was a small electronic inefficiency in the spectrometer owing to dead time, probably introduced by the pile-up rejectors. This effect was monitored by injecting into the preamplifiers pulses of constant energy. The pulses were made by pulse generators triggered in coincidence with every thousandth K_{stop}(reg'd). The energy of the injected pulses was outside the limits of the expected range of x-ray lines, usually near the high end of the amplifier output capability. However, some tests were made with the energy of the pulse generators set near to the noise threshold. This was done with a low-Z element to verify that low-energy x rays were not being missed. We assumed that the electronic efficiency was given by

$$\epsilon = 1000N_{PG}/K_{\text{stop}}\ (\text{reg'd}),$$

where N_{PG} was the number of events recorded in the "spectral line" made by the pulse generator. Values of ϵ were around 0.9.

The pulse generator peaks were not included in the illustrations of the spectra because of their large amplitudes.

IV. CALIBRATION

One of the objects of the experiment was to determine the absolute intensities, I, of the x-ray lines defined by

$$I(n_i \to n_f) = N_x/(0.70 \times 1000 N_{PG} \times T \times \eta),$$

where $n_i \to n_f$ designates the kaonic transition, N_x was the number of x rays in the spectral line, T was the transmission of the target, and η was the efficiency of the detector including solid angle.

The numbers of x rays in the spectral lines were determined by a computer program that counted the events in each peak. A more complete discussion is given later.

Some of the x rays were absorbed by the target material in which the kaons stopped. Therefore, it was necessary to know the transmission of each target for the x-ray energy of the line under consideration. X-ray absorption coefficients were taken from a compilation of x-ray cross sections, by McMaster *et al.*[15] Because the geometry of our targets and detectors was rather poorly defined, we used only the sum of the photoelectric and incoherent cross sections.

We assumed that equal numbers of kaons stopped in equal-depth intervals as they penetrated the targets. Under this assumption, target transmission is given by

$$T = [(\mu/\rho)t]^{-1}[1 - e^{-\mu/\rho t}],$$

where μ/ρ is the absorption coefficient in $\mathrm{cm^2\,g^{-1}}$ and t is the thickness in $\mathrm{g\,cm^{-2}}$ as seen by the detector. The range curve of Fig. 4 shows that kaons stop reasonably uniformly in targets about 3 $\mathrm{g\,cm^{-2}}$ thick. We are especially interested in the intensities of the highest-energy lines of each spectrum. In our targets, x-ray transmission of the highest observable energy amounted to about 0.8 and was almost independent of Z. As Z increased the energy of the last observable transitions also increased in a way to keep the target transparency about constant.

Calibration of the efficiency of the detectors to register x rays was determined by using sets of sources standardized by the International Atomic Energy Agency. Detectors were routinely calibrated by placing a standard source at the position normally occupied by the geometrical centers of the target. The efficiency η was assumed to be given by

$$\eta = N_x/N_s R_B,$$

where N_x was the number of x rays registered in a spectral line per second of system live time, N_s was the source strength in disintegrations per second, and R_B was the source branching ratio (the ratio of the number of photons emitted at a discrete energy to the number of total disintegrations). For x-ray lines of energy less than about 15 keV it was important to correct for the absorption of the source holder and in some cases for the absorption of the source material itself. A plot of η versus photon energy is shown for two of the detectors in Fig. 5. Probably the weakest assumption in this procedure was that the source position actually corresponded to the center of the distribution of stopped kaons. We had no way of monitoring the effective kaon distribution. By placing calibration sources at different positions than the geometrical center of the targets, we established that the maximum error could be expected to be less than $\pm 5\%$ owing to uncertainties in the beam kaon distribution. In many instances intensities were measured simultaneously by two detectors, one on each side of the beam. The quality of agreement between these determinations gave us confidence in the measurements.

Several standard radioactive sources were used for efficiency and energy calibrations. Data on the energies of the emitted radiations were mostly taken from Lederer *et al.*[16]

Calibration spectra for efficiency and energy were made two or three times per day during periods of beam-off. The spectrometer was activated by relinquishing the requirement that a kaon stop signal be in coincidence with a detector signal. Linear gates and other circuits sensitive to pulse height were undisturbed. We elected to make separate spectra for energy calibrations instead of allowing calibration lines to leak onto the kaonic x-ray spectra. We did not want to purposely introduce events extraneous to kaon-induced lines for fear of covering over unexpected weak lines such as nuclear γ rays. By this procedure, we gave up the effective averaging that compensates for drift in circuits sensitive to pulse heights. With

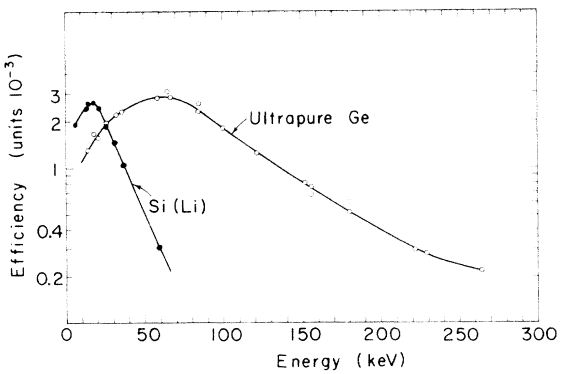

FIG. 5. Plots of detector efficiencies vs photon energy. Standard sources of ^{241}Am, ^{57}Co, ^{137}Cs, and ^{182}Ta were used to make the calibrations.

TABLE III. Numbers pertinent to the spectra of Fig. 6. Events recorded were those comprised of a K_{stop} (reg) pulse in coincidence with a detector discriminator pulse that had been passed by the pile-up rejector. For definitions of K_{beam} and K_{stop}, see text.

Spectrum and (detector)	Bevatron bursts	S_3 (pions) (10^6)	K_{beam} (10^6)	K_{stops}(true) (10^6)	Events recorded
CCl_4 (148)	31 160	4345	17.901	3.63	41 390
S (58A)	49 622	7367	33.830	7.81	211 245

our modest beam intensity, there were no measurable rate-sensitive effects. However, there were slight drifts in energy that prevented us from making a more accurate measurement of the kaon mass than the presently accepted value.

Energies of the spectral lines were determined by using a computer to find the pulse-height centroids of the calibration and unknown lines. The centroids of the standard lines were used to make energy versus pulse-height functions that were not exactly linear in all cases.

V. OPERATION AND ANALYSIS

Routine operations consisted of loading the target wheel with a series of elements or isotopes and exposing each sample in turn to the beam for periods of about 6 h. Each target accumulated about 48 h of beam time. The target wheel contained up to seven samples. It was remotely controlled from the counting area where its position was monitored by a binary-encoder device whose readout was recorded along with the run number. At the end of each 6-h period the readouts of

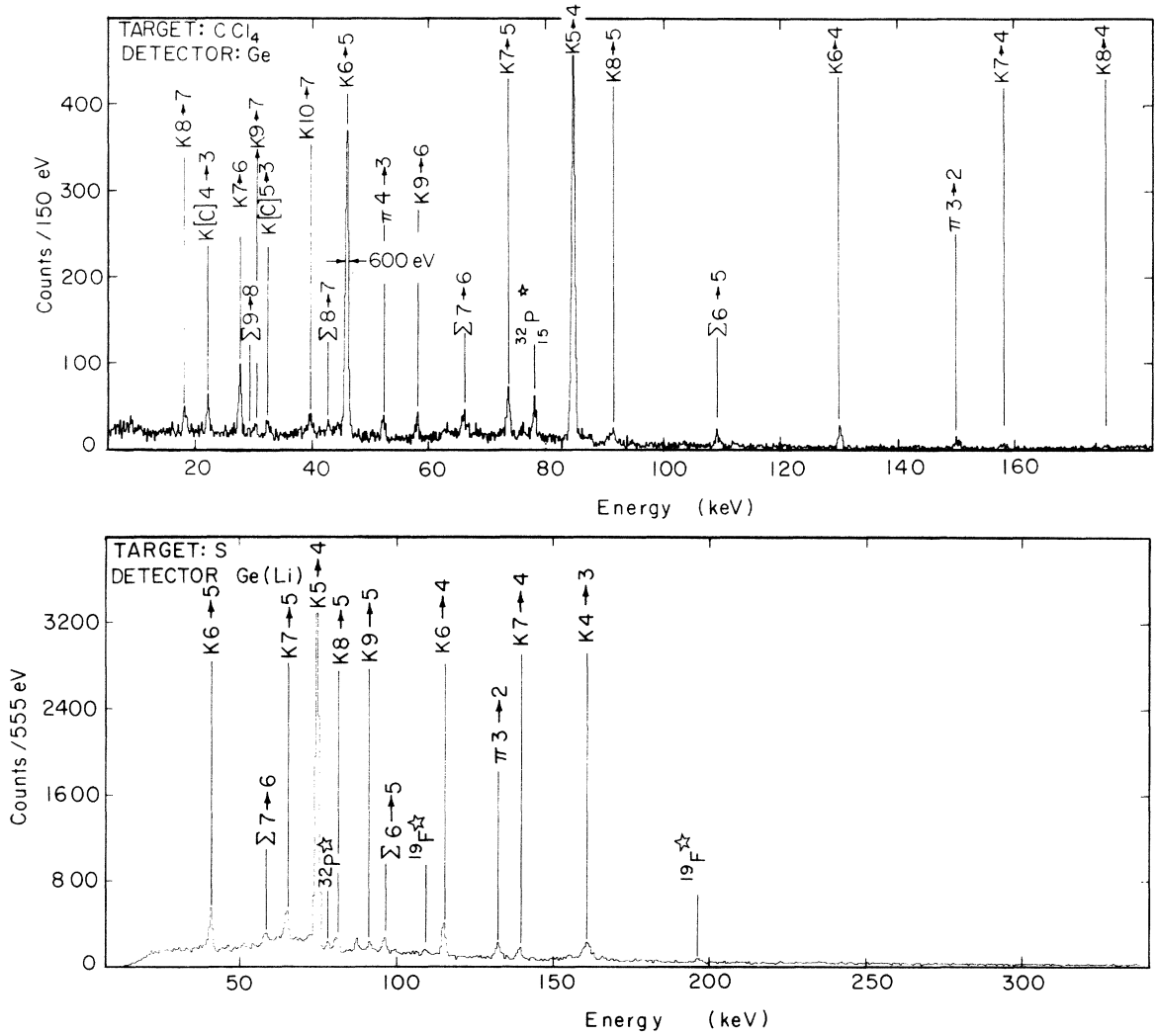

FIG. 6. Kaonic x-ray spectra of CCl_4 and S. The line at 78 keV is attributed to nuclear γ rays from the first excited level of $^{32}_{15}$P. In the spectrum of S the lines at 110 and 197 keV correspond to the first excited states of $^{19}_{9}$F.

several electronic pulse scalers were recorded for both bookkeeping and diagnostic purposes. Included in the numbers recorded were those examples in Table III.

At appropriate intervals the data tapes were processed at the LBL Computer Center. For each spectrum the number of events in each pulse-height channel was printed out. In addition the computer's plotter made graphs, e.g., Fig. 6.

Individual spectra were examined and lines identified by their energies. For most of the spectra the number of x rays represented by the peaks were determined by a computer program that counted the number of events in each line and subtracted the background. For each line the computer was assigned by eye the sections (in channel numbers) over which to evaluate the events and the background. Usually the background was determined from a group of appropriate channels on each side of the line by projecting the average number of counts per channel linearly under the peak. For each line it was instructed to measure, the computer printed out the net number of x rays and an error based on the sum of the peak and background counts. The centroids of the lines were also calculated and tabulated. The computer thus performed much of the bookkeeping chores and hopefully eliminated a significant amount of human subjectivity.

The broadened and shifted lines of the spectra of high statistical accuracy were handled in a more refined manner. It was assumed that the distribution of x rays in sharp lines was due to statistics and random electronic noise and was, therefore, Gaussian. Broadened lines were assumed to be Lorentzian in distribution. Observed line shapes were then products of two distributions. Shape parameters of instrument-broadened lines were obtained from sharp kaonic lines near in energy to the line under investigation. A computer program was employed to obtain the best fit to the broadened lines under the above assumptions.

VI. RESULTS

A. Kaonic atoms

Most of the results of the experiment are contained in Table IV which is a catalog of the observed kaonic x-ray lines. The first column designates the target. Where pure isotopes were used, A is specified by a left-hand superscript. Where compounds were used, the listed lines are those of the underlined element. For example, $Na^{35}\underline{Cl}$ signifies that the target was sodium chloride and the listed lines are from chlorine 35. Column 2 indicates initial to final principal-quantum-number transitions. Column 3 contains the calculated Coulomb energies of the transitions to orbits of maximum angular momenta. The energies consist of the Klein-Gordon value plus corrections for vacuum polarization and finite size of the nuclear charge. Column 4 lists the intensities of the lines in x rays per kaon stopped in the targets. Column 5 contains $\Delta I/I$ where ΔI consists of statistical errors in the numbers of x rays in the peaks and backgrounds. Column 6 gives our estimate of the errors in absolute intensities. It contains an additional error component of ±15%; 10% came from uncertainties in the numbers of kaons stopped and an estimated 10% from uncertainties in electronic efficiencies, detector efficiencies, and target absorption.

Intensities versus Z are plotted for principal lines in Fig. 7. In assigning intensities to lines from elements in compounds, we did not account for the numbers of kaons that were captured by atoms of the constituent elements. Fermi and Teller[17] predicted that mesons should be captured approximately in proportion to Z. Studies of muonic and pionic atoms show considerable deviation from the Z rule and kaonic atoms probably also depart from the Fermi-Teller prediction. Accordingly, we give the intensities in proportion to the observed number of x rays in each peak divided by the number of kaons stopped in the targets whether or not the targets consisted of elements or compounds. Therefore, the intensities of some of the lines of elements measured in compounds appear to be low, for example, Br in AgBr. Concerning elements measured as pure isotopes, we have plotted in Fig. 7 the average intensities of the measured isotopes making no effort to reconstitute the natural isotopic abundances.

For all but a few of the lines we can distinguish the principal quantum numbers of the transitions by the energy of the x rays. Some exceptions are the transitions $n=8$ to $n=6$ that have almost the same energy as the transitions $n=6$ to $n=5$. In Table IV asterisks were inserted in front of appropriate $n=*6\rightarrow 5$ to indicate that the intensities $n=6\rightarrow 5$ and $n=8\rightarrow 6$ had been summed. Usually $\Delta n=-2$ transitions have about 0.1 the intensity of the principal lines. Figure 8 shows x rays per stopped kaon versus Z for $n=7\rightarrow 5$ transitions.

We could not distinguish angular momentum states for any of the transitions.

In Table IV are listed the calculated energies of the lines. The values are for reference only and it is not to be construed that all the lines we measured had exactly the listed energy. (A discussion of shifted and broadened lines appears later in this section.) For energy evaluation, the kaon mass was taken to be 493.84 MeV. Vacuum

TABLE IV. Measured intensities of observed kaonic x-ray lines. Column 1 lists the targets used in the experiment. Atomic weights are shown as superscripts for targets that were practically pure isotopes. In chemical compounds, x rays listed are those of the element underlined. Column 2 contains principal quantum numbers of the initial and final states. Asterisks that precede $n = 6 \rightarrow 5$ transitions indicate that intensities of $n = 8 \rightarrow 6$ transitions are included because the energies are almost equal. In Column 3 are listed the electromagnetic transition energies. Intensities in x rays per kaon stopped in the target are listed in Column 4. Column 5 contains errors, $\Delta I/I$, due mainly to uncertainties in the numbers of x rays in the spectral lines and should be used to compare intensities in the same element. In Column 6 are listed estimated errors in absolute intensity.

Target A_Z	Transition n_i	n_f	Calculated transition energy (keV)	I x rays per K_{stop}	$\pm\Delta I/I$ Use for error in relative I	$\pm\Delta I$ Use for error in absolute I
^{4}He	3	2	6.463	0.092	0.22	0.025
	4	2	8.722	0.052	0.20	0.013
	5	2	9.767	0.024	0.25	0.007
^{6}Li	5	3	7.743	0.011	0.25	0.003
	3	2	15.157	0.14	0.08	0.02
	4	2	20.450	0.031	0.12	0.006
	5	2	22.899	0.011	0.20	0.003
^{7}Li	5	3	7.828	0.015	0.20	0.004
	3	2	15.323	0.15	0.08	0.03
	4	2	20.674	0.034	0.10	0.006
	5	2	23.150	0.016	0.20	0.004
^{9}Be	4	3	9.680	0.21	0.20	0.05
	5	3	14.155	0.045	0.33	0.017
	3	2	27.717	0.11	0.23	0.03
^{10}B	4	3	15.220	0.14	0.11	0.03
	5[a]	3	22.252	0.063	0.18	0.015
	3	2	43.582	0.088	0.39	0.037
^{11}B	4	3	15.289	0.19	0.08	0.03
	5[a]	3	22.353	0.066	0.19	0.016
	3	2	43.781	0.074	0.73	0.055
^{12}C	6	4	15.765	0.029	0.30	0.011
	4	3	22.112	0.36	0.05	0.06
	5	3	32.328	0.070	0.15	0.014
	6	3	37.874	0.028	0.25	0.008
	3	2	63.321	0.028	0.25	0.008
$H_2{}^{16}\underline{O}$	6*	5	9.972	0.27	0.33	0.10
	7	5	15.979	0.020	0.55	0.011
	5	4	18.377	0.13	0.10	0.02
	6	4	28.344	0.031	0.18	0.007
	7	4	34.352	0.014	0.31	0.005
	4	3	39.766	0.15	0.04	0.02
	5	3	58.133	0.034	0.08	0.006
	6	3	68.104	0.022	0.10	0.004
	7	3	74.115	0.014	0.13	0.003
	8	3	78.015	0.006	0.24	0.002
$^{23}\underline{Na}$Cl	5	4	35.120	0.18	0.05	0.03
	6	4	54.163	0.017	0.21	0.004
	4	3	76.014	0.16	0.04	0.02
Mg	5	4	41.859	0.42	0.15	0.09
	6	4	64.555	0.034	0.20	0.009
	4	3	90.606	0.24	0.12	0.04

TABLE IV *(continued)*

Target A_Z	Transition n_i	n_f	Calculated transition energy (keV)	I x rays per K_{stop}	$\pm\Delta I/I$ Use for error in relative I	$\pm\Delta I$ Use for error in absolute I
Si	5	4	57.178	0.36	0.07	0.06
	6	4	88.175	0.036	0.20	0.008
	4	3	123.780	0.13	0.08	0.02
^{31}P	4	3	142.367	0.077	0.12	0.015
	5	4	65.760	0.34	0.05	0.06
	6	4	101.406	0.024	0.26	0.007
	7	4	122.890	0.012	0.46	0.006
S	9	6	51.197	0.008	0.24	0.002
	7	6	24.467	0.24	0.09	0.04
	6*	5	40.619	0.36	0.02	0.06
	7	5	65.070	0.040	0.05	0.006
	8	5	80.934	0.013	0.10	0.002
	9	5	91.808	0.006	0.17	0.001
	5	4	74.883	0.36	0.02	0.06
	6	4	115.471	0.039	0.05	0.006
	7	4	139.933	0.015	0.10	0.003
	8	4	155.804	0.006	0.25	0.002
	4	3	162.127	0.047	0.06	0.008
CCl_4	8	7	17.944	0.51	0.21	0.13
	9	7	30.237	0.035	0.43	0.016
	10	7	39.023	0.031	0.29	0.010
	7	6	27.669	0.26	0.10	0.05
	9	6	57.895	0.016	0.18	0.004
	6*	5	45.936	0.29	0.03	0.04
	7	5	73.586	0.037	0.06	0.006
	8	5	91.526	0.013	0.11	0.002
	9	5	103.822	0.007	0.22	0.002
	5	4	84.689	0.36	0.01	0.06
	6	4	130.589	0.036	0.05	0.006
	7	4	158.252	0.013	0.12	0.002
	8	4	176.199	0.011	0.24	0.003
	4	3	183.366	0.039	0.08	0.007
$Na^{35}Cl$	7	6	27.663	0.11	0.20	0.03
	6*	5	45.926	0.17	0.06	0.03
	7	5	73.571	0.010	0.50	0.005
	8	5	91.508	0.010	0.31	0.004
	5	4	84.672	0.17	0.03	0.03
	6	4	130.562	0.021	0.15	0.004
$Na^{37}Cl$	7	6	27.686	0.17	0.14	0.03
	6*	5	45.964	0.18	0.05	0.03
	7	5	73.631	0.020	0.27	0.006
	8	5	91.582	0.010	0.28	0.004
	5	4	84.740	0.18	0.03	0.03
	6	4	130.668	0.020	0.13	0.004
K	7	5	92.079	0.027	0.29	0.009
	5	4	105.985	0.25	0.05	0.04
	6	4	163.418	0.025	0.33	0.009
Ti	7	6	46.556	0.15	0.35	0.06
	6*	5	77.304	0.19	0.07	0.03
	7	5	123.821	0.024	0.34	0.009
	5	4	142.549	0.16	0.08	0.03
^{51}V	7	6	50.926	0.067	0.35	0.025
	9	6	106.540	0.020	0.35	0.008

TABLE IV *(continued)*

Target A_Z	Transition n_i	n_f	Calculated transition energy (keV)	I x rays per K_{stop}	$\pm\Delta I/I$ Use for error in relative I	$\pm\Delta I$ Use for error in absolute I
^{51}V	10	6	122.714	0.014	0.57	0.008
	6*	5	84.563	0.12	0.10	0.02
	7	5	135.444	0.018	0.48	0.009
	5	4	155.941	0.10	0.11	0.02
Cr	7	6	55.472	0.099	0.30	0.033
	6*	5	92.113	0.14	0.06	0.02
	7	5	147.533	0.010	0.85	0.009
	5	4	169.872	0.067	0.10	0.012
^{55}Mn	7	6	60.232	0.057	0.48	0.029
	6*	5	100.021	0.10	0.09	0.02
	7[b]	5	160.196	0.032	0.23	0.009
	5	4	184.465	0.064	0.15	0.014
Fe	7	6	65.168	0.077	0.25	0.022
	6*	5	108.220	0.12	0.07	0.02
	7	5	173.323	0.041	0.32	0.014
	5	4	199.595	0.064	0.19	0.015
^{59}Co	7	6	70.323	0.096	0.13	0.019
	6*	5	116.783	0.11	0.07	0.02
	5	4	215.400	0.077	0.15	0.016
^{58}Ni	8	7	49.036	0.13	0.49	0.06
	7	6	75.629	0.094	0.10	0.017
	6*	5	125.599	0.13	0.05	0.02
	7	5	201.148	0.018	0.52	0.010
	5	4	231.671	0.045	0.24	0.012
^{60}Ni	7	6	75.651	0.097	0.16	0.021
	6*	5	125.636	0.15	0.08	0.03
	5	4	231.739	0.033	0.41	0.014
^{62}Ni	7	6	75.672	0.091	0.10	0.016
	6*	5	125.672	0.16	0.04	0.02
	7	5	201.264	0.028	0.36	0.011
	5	4	231.805	0.047	0.18	0.011
^{63}Cu	8	7	52.646	0.15	0.48	0.07
	7	6	81.198	0.16	0.08	0.03
	9	6	169.842	0.020	0.34	0.008
	6*	5	134.852	0.22	0.05	0.04
	7	5	215.961	0.028	0.30	0.009
	5	4	248.751	0.061	0.22	0.016
^{65}Cu	8	7	52.659	0.11	0.35	0.04
	7	6	81.218	0.17	0.08	0.03
	9	6	169.885	0.022	0.55	0.013
	6*	5	134.886	0.23	0.05	0.04
	7	5	216.015	0.044	0.36	0.017
	5	4	248.813	0.070	0.21	0.018
Zn	8	7	56.363	0.14	0.18	0.03
	9	7	94.941	0.040	0.14	0.008
	7	6	86.934	0.26	0.04	0.04
	6*	5	144.383	0.31	0.02	0.05
	7	5	231.218	0.036	0.22	0.010
	5	4	266.345	0.049	0.21	0.013
Ge	10	8	75.384	0.064	0.30	0.021

TABLE IV *(continued)*

Target A_Z	Transition n_i	n_f	Calculated transition energy (keV)	I x rays per K_{stop}	$\pm\Delta I/I$ Use for error in relative I	$\pm\Delta I$ Use for error in absolute I
Ge	8	7	64.197	0.23	0.14	0.05
	9	7	108.132	0.062	0.16	0.014
	7	6	99.020	0.36	0.04	0.06
	6*	5	164.467	0.49	0.04	0.08
	7	5	263.367	0.060	0.36	0.023
Se	10	8	85.168	0.068	0.19	0.017
	8	7	72.533	0.30	0.08	0.05
	9	7	122.169	0.062	0.15	0.013
	7	6	111.883	0.45	0.03	0.07
	6*	5	185.843	0.50	0.03	0.08
	7	5	297.582	0.048	0.30	0.016
AgBr	8	7	76.882	0.18	0.20	0.04
	7	6	118.594	0.14	0.10	0.02
	6*	5	196.997	0.13	0.10	0.02
Mo	9	8	75.972	0.15	0.21	0.04
	8	7	110.924	0.21	0.08	0.04
	7	6	171.132	0.21	0.07	0.03
	6*	5	284.342	0.11	0.17	0.02
^{103}Rh	10	9	62.373	0.19	0.39	0.08
	11	9	108.443	0.035	0.41	0.015
	9	8	87.273	0.20	0.12	0.04
	10	8	149.573	0.050	0.21	0.013
	8	7	127.430	0.21	0.07	0.04
	7	6	196.613	0.22	0.07	0.04
	6*	5	326.720	0.19	0.19	0.05
AgBr	9	8	95.249	0.12	0.19	0.03
	8	7	139.082	0.13	0.09	0.02
	7	6	214.601	0.13	0.09	0.02
^{107}Ag	12	10	88.543	0.072	0.44	0.034
	10	9	68.066	0.19	0.24	0.06
	11	9	118.337	0.057	0.20	0.014
	9	8	95.241	0.19	0.10	0.04
	10	8	163.224	0.029	0.39	0.012
	8	7	139.070	0.27	0.05	0.04
	9	7	234.179	0.058	0.35	0.022
	7	6	214.584	0.26	0.06	0.04
	6*	5	356.612	0.15	0.19	0.04
^{109}Ag	10	9	68.072	0.14	0.36	0.05
	11	9	118.348	0.068	0.19	0.017
	9	8	95.250	0.21	0.10	0.04
	10	8	163.239	0.043	0.24	0.012
	8	7	139.038	0.28	0.05	0.04
	9	7	234.201	0.038	0.43	0.017
	7	6	214.604	0.28	0.06	0.05
	6*	5	356.645	0.14	0.19	0.03
Cd	10	9	71.017	0.076	0.32	0.028
	11	9	123.466	0.032	0.23	0.009
	9	8	99.372	0.14	0.09	0.02
	10	8	170.300	0.041	0.28	0.013
	8	7	145.104	0.25	0.05	0.04
	9	7	244.334	0.057	0.25	0.017
	7	6	223.900	0.28	0.06	0.05

TABLE IV *(continued)*

Target A_Z	Transition n_i	Transition n_f	Calculated transition energy (keV)	I x-rays per K_{stop}	$\pm\Delta I/I$ Use for error in relative I	$\pm\Delta I$ Use for error in absolute I
Cd	6*	5	372.110	0.18	0.21	0.05
Sn	10	9	77.092	0.20	0.22	0.05
	11	9	134.023	0.038	0.38	0.015
	9	8	107.875	0.32	0.07	0.05
	10	8	184.866	0.079	0.19	0.019
	8	7	157.527	0.38	0.05	0.06
	8	6	400.333	0.048	0.55	0.028
	6	5	404.023	0.076	0.33	0.027
^{127}I	10	9	86.670	0.32	0.17	0.07
	11	9	150.666	0.052	0.29	0.017
	9	8	121.282	0.36	0.08	0.06
	8	7	177.114	0.41	0.06	0.07
	9	7	298.201	0.065	0.34	0.024
	7	6	273.331	0.33	0.08	0.06
$^{142}Nd_2O_3$	12	10	144.602	0.025	0.52	0.014
	10	9	111.197	0.20	0.16	0.04
	9	8	155.619	0.15	0.13	0.03
	8	7	227.291	0.18	0.11	0.03
	7	6	350.843	0.11	0.23	0.03
$^{144}Nd_2O_3$	11	10	82.208	0.21	0.39	0.09
	12	10	144.610	0.049	0.40	0.021
	10	9	111.202	0.19	0.19	0.05
	9	8	155.627	0.19	0.12	0.04
	8	7	227.303	0.22	0.10	0.04
	7	6	350.861	0.23	0.18	0.05
$^{146}Nd_2O_3$	10	9	111.208	0.28	0.15	0.06
	9	8	155.635	0.18	0.13	0.04
	8	7	227.315	0.19	0.12	0.04
	7	6	350.878	0.15	0.22	0.04
$^{147}Sm_2O_3$	11	10	87.801	0.16	0.24	0.04
	12	10	154.443	0.038	0.44	0.018
	10	9	118.770	0.20	0.11	0.04
	11	9	206.439	0.049	0.38	0.020
	9	8	166.224	0.20	0.09	0.04
	8	7	242.790	0.21	0.09	0.04
	7	6	374.791	0.20	0.15	0.04
$^{148}Sm_2O_3$	11	10	87.803	0.18	0.20	0.04
	12	10	154.447	0.067	0.29	0.022
	10	9	118.773	0.19	0.09	0.03
	11	9	206.444	0.095	0.37	0.038
	9	8	166.228	0.23	0.06	0.04
	8	7	242.796	0.24	0.06	0.04
	7	6	374.800	0.21	0.11	0.04
$^{149}Sm_2O_3$	11	10	87.805	0.21	0.18	0.05
	10	9	118.776	0.21	0.10	0.04
	11	9	206.449	0.035	0.38	0.014
	9	8	166.232	0.18	0.09	0.03
	10	8	284.805	0.045	0.54	0.025
	8	7	242.802	0.23	0.09	0.04
	7	6	374.809	0.18	0.18	0.04

TABLE IV *(continued)*

Target A_Z	Transition n_i	n_f	Calculated transition energy (keV)	I x-rays per K_{stop}	$\pm\Delta I/I$ Use for error in relative I	$\pm\Delta I$ Use for error in absolute I
$^{152}Sm_2O_3$	11	10	87.811	0.20	0.26	0.06
	12	10	154.462	0.039	0.50	0.020
	10	9	118.785	0.22	0.13	0.04
	9	8	166.244	0.18	0.11	0.03
	8	7	242.819	0.30	0.08	0.05
	7	6	374.836	0.16	0.19	0.04
$^{154}Sm_2O_3$	11	10	87.815	0.18	0.39	0.08
	10	9	118.790	0.23	0.14	0.05
	9	8	166.251	0.23	0.09	0.04
	8	7	242.830	0.21	0.11	0.04
	7	6	374.852	0.18	0.19	0.04
$^{156}Gd_2O_3$	11	10	93.591	0.074	0.58	0.044
	10	9	126.607	0.24	0.12	0.05
	11	9	220.051	0.059	0.43	0.027
	9	8	177.196	0.17	0.12	0.03
	8	7	258.828	0.19	0.15	0.04
	7	6	399.576	0.15	0.32	0.05
$^{157}Gd_2O_3$	11	10	93.593	0.12	0.20	0.03
	10	9	126.609	0.16	0.09	0.03
	11	9	220.056	0.045	0.37	0.018
	9	8	177.200	0.14	0.10	0.03
	8	7	258.834	0.17	0.12	0.03
	7	6	399.584	0.11	0.40	0.05
$^{158}Gd_2O_3$	11	10	93.595	0.15	0.36	0.06
	10	9	126.612	0.21	0.12	0.04
	9	8	177.204	0.17	0.12	0.03
	8	7	258.839	0.21	0.13	0.04
	7	6	399.593	0.0[illegible]	0.51	0.048
$^{167}Er_2O_3$	11	10	105.714	0.2[illegible]	0.22	0.06
	10	9	143.013	0.2[illegible]	0.13	0.04
	9	8	200.170	0.21	0.10	0.04
	8	7	292.413	0.21	0.13	0.04
$^{170}Er_2O_3$	11	10	105.720	0.15	0.26	0.05
	10	9	143.021	0.27	0.08	0.05
	9	8	200.182	0.20	0.10	0.04
	8	7	292.430	0.20	0.11	0.04
^{181}Ta	12	11	92.649	0.27	0.37	0.11
	11	10	121.912	0.32	0.18	0.08
	10	9	164.936	0.37	0.12	0.07
	9	8	230.875	0.23	0.15	0.0[illegible]
	8	7	337.308	0.26	0.19	0.06
W	12	11	95.216	0.2[illegible]	0.46	0.1
	11	10	125.291	0.1[illegible]	0.25	0
	10	9	169.510	0.33	0.11	0 6
	9	8	237.282	0.27	0.11	5
	8	7	346.677	0.32	0.13	06
Ir	12	11	103.128	23	0.26	0.07
	11	10	135.707	0.17	0.17	0.04
	10	9	183.608	0.21	0.12	0.04
	9	8	257.031	0.18	[illegible]	0.04
	8	7	375.560	0.18	0.18	0.04

TABLE IV *(continued)*

Target A_Z	Transition n_i	n_f	Calculated transition energy (keV)	I x-rays per K_{stop}	$\pm\Delta I/I$ Use for error in relative I	$\pm\Delta I$ Use for error in absolute I
^{197}Au	12	11	108.579	0.25	0.40	0.11
	11	10	142.882	0.16	0.28	0.05
	10	9	193.321	0.21	0.16	0.05
	9	8	270.637	0.26	0.15	0.05
	8	7	395.462	0.25	0.20	0.06
$^{203}\underline{Tl}_2O_3$	12	10	264.201	0.051	0.53	0.029
	11	10	150.246	0.15	0.28	0.05
	10	9	203.290	0.29	0.14	0.06
	9	8	284.603	0.20	0.18	0.05
	8	7	415.892	0.19	0.25	0.06
$^{205}\underline{Tl}_2O_3$	12	11	114.175	0.18	0.36	0.07
	11	10	150.250	0.15	0.24	0.04
	10	9	203.295	0.27	0.14	0.06
	9	8	284.610	0.27	0.15	0.06
	8	7	415.903	0.22	0.26	0.06
Pb	15	14	58.186	0.13	0.30	0.05
	16	14	105.726	0.046	0.48	0.023
	15	13	130.269	0.053	0.38	0.022
	13	12	91.004	0.17	0.24	0.05
	14	12	163.056	0.074	0.19	0.018
	15	12	221.182	0.026	0.41	0.011
	12	11	117.024	0.24	0.10	0.04
	11	10	154.000	0.29	0.06	0.05
	10	9	208.371	0.32	0.05	0.05
	11	9	362.032	0.031	0.41	0.013
	9	8	291.723	0.31	0.05	0.05
	8	7	426.308	0.27	0.08	0.05
^{209}Bi	15	14	59.619	0.32	0.29	0.10
	13	12	93.245	0.24	0.31	0.08
	14	12	167.070	0.099	0.33	0.036
	12	11	119.907	0.37	0.14	0.08
	11	10	157.796	0.36	0.10	0.07
	12	10	277.467	0.072	0.44	0.034
	10	9	213.511	0.45	0.07	0.08
	9	8	298.923	0.44	0.08	0.07
	8	7	436.843	0.44	0.10	0.08
^{232}Th	15	14	70.144	0.17	0.56	0.10
	14	13	86.997	0.29	0.20	0.07
	12	11	141.096	0.21	0.33	0.08
	11	10	185.693	0.18	0.30	0.06
	10	9	251.283	0.37	0.13	0.07
	9	8	351.856	0.27	0.19	0.07
	8[c]	7	514.290	0.24	0.30	0.12
^{238}U	15	14	73.308	0.45	0.33	0.16
	12	11	147.467	0.32	0.25	0.09
	11	10	194.083	0.34	0.18	0.08
	10	9	262.645	0.28	0.17	0.06
	9	8	367.780	0.29	0.19	0.07

[a] ^{10}B and ^{11}B transitions $n = 5 \rightarrow 3$ include background from C degrader $n = 4 \rightarrow 3$ which amounts to about 0.03.

[b] Mn $n = 7 \rightarrow 5$ possibly includes ^{47}Ti nuclear γ rays.

[c] Th $n = 8 \rightarrow 7$ intensity was estimated owing to interference from annihilation radiation.

polarization corrections to first order were included as well as corrections for finite nuclear sizes which were taken to be uniform in charge distribution. For pure isotopes the accepted value of the atomic mass was used. In natural-abundance targets, the average atomic mass was used for energy calculations.

Additional comments on Table IV are as follows.

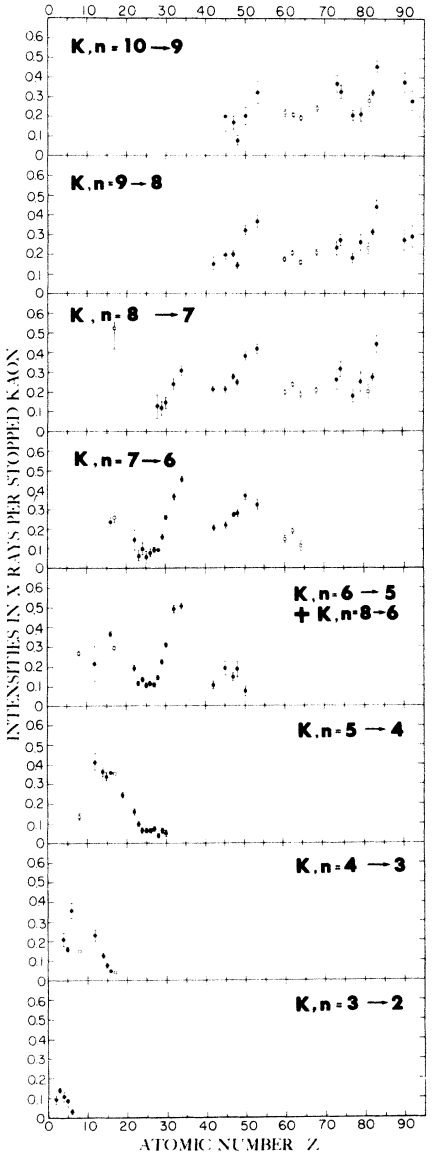

FIG. 7. Intensity vs Z of the observed principal ($\Delta n = -1$) kaonic x-ray lines up through $n = 10 \rightarrow 9$. Error bars include statistical uncertainties in x-ray counts, but no errors were included for the absolute numbers of stopped kaons which could amount to ±15%. Filled-in circles apply to targets of elements; squares to chemical compounds where intensities refer to x rays per kaon stopped in the entire compound.

We have listed all the lines that we observed that corresponded in energy to kaonic transitions. There are instances in which transitions, presumably not subject to nuclear absorption, appeared in one or two isotopes but not in all isotopes of the same element. For example, in ^{58}Ni the transition $n = 8 \rightarrow 7$ appeared but it is missing in ^{60}Ni and ^{62}Ni; the transition $n = 11 \rightarrow 9$ was observed in ^{156}Gd and ^{157}Gd but not in ^{158}Gd. We have no explanation for such occurrences. Some principal lines of the heavy elements are missing from the table owing to interference from electronic K_α and K_β x rays. The observed K_α and K_β lines were apparently due to the fluorescence because they were x rays characteristic of the target atoms and not $Z_{\text{target}} - 1$ as would be expected if the x rays originated in the atoms in which kaons stopped.

When the experiment was being planned, it was decided that we would compare the x-ray intensities of the same transitions in different isotopes of the same elements. The idea was to choose elements in which the last observable transition underwent strong nuclear absorption, for instance, $n = 5 \rightarrow 4$ in Ni. If kaonic absorption were strongly dependent on the number of neutrons near the nuclear surface, the x-ray intensity might be weakened by the addition of neutrons. We tried ^{58}Ni, ^{60}Ni, and ^{62}Ni with no measurable effect on the intensities as revealed by inspection of Table IV. The same remarks can be made about isotopes of Li, B, Cl, Cu, Ag, Nd, Sm, Gd, Er, and Tl. Apparently the effective nuclear radius as probed by the kaons does not change appreciably for different isotopes, at least within the accuracy of our observations. In the rare-earth elements the effect could have been enhanced because additional neutrons cause the nuclei to be deformed and to take on quadrupole moments. Again there was no significant effect on the intensities of the x rays.

In order to show the behavior of the intensities near cutoff, Fig. 9 presents several plots of the intensity ratios of consecutive transitions versus Z.

For a given transition, $n \rightarrow n - 1$, Fig. 10 shows,

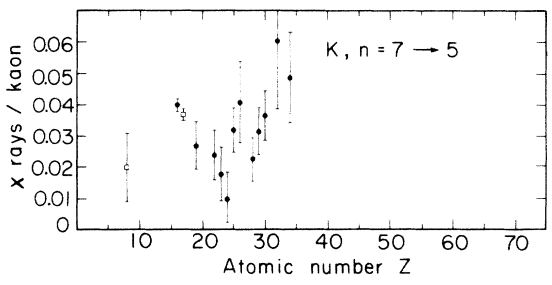

FIG. 8. Intensities of kaonic x-ray lines for transitions $n = 7 \rightarrow 5$.

for increasing Z, the first element at which the x-ray transition fell below the limits of detectability. Data on kaonic and hyperonic x rays came from the present experiment. Pionic x-ray data were taken from Kunselman.[21] These empirical curves may be useful for predicting the last observable Σ^- hyperonic lines in heavy elements.

Some of the kaonic x-ray lines are broadened and shifted in energy due to strong interaction effects. Figure 11 illustrates an example. Table V presents a list of the characteristics of such lines observed mostly by the CERN group.[18] Linewidth is a measure of the absorption rate. Energy-level shifts are ordinarily calculated by perturbation theory using complex scattering lengths, but the unusually high absorption rate encountered in kaonic atoms also has an influence on the energy levels. References to papers that discuss these problems are given in Sec. VII.

Figure 7 shows that the intensities of the x-ray emission undergo remarkable variations as the atomic number changes. Among the data, one of the most striking examples occurs for $n=6$ to $n=5$ transitions in the region $Z=16$ to $Z=34$. At $Z=16$ the intensity is about 0.4 x rays per kaon stop. It then drops drastically to 0.1 around $Z=25$ and climbs back to about 0.4 at $Z=34$. The $n=7$ to $n=6$ transitions make similar excursions over the same range in Z. The behavior of the intensities suggests that maxima occur near closed atomic electron shells.

For $n=5$ to $n=4$ transitions, the disappearance of x rays around $Z=32$ is attributed to the encounter of kaons with nuclear matter. However, the $n=6$ to $n=5$ x rays are near maximum intensity at $Z=34$ and do not disappear until Z exceeds 50. The same effect of minimum intensity around

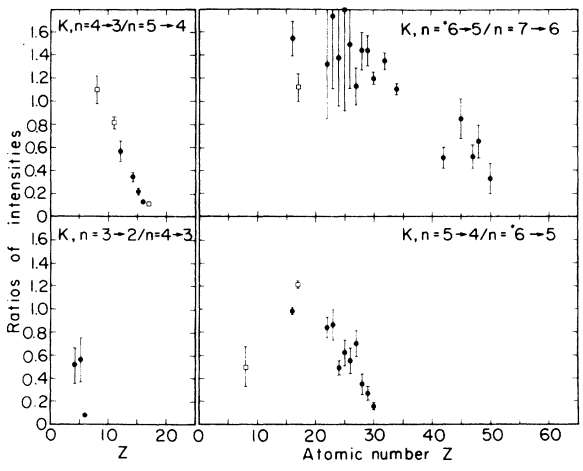

FIG. 9. Ratios of the intensities of consecutive kaonic transitions vs Z.

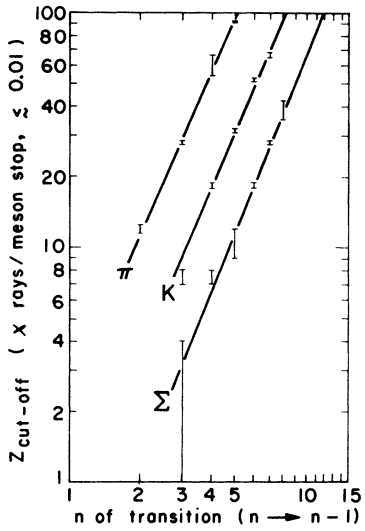

FIG. 10. As Z increases, $Z_{\text{cut-off}}$ is the first Z at which a given transition fell below the limits of detectability. The errors are due to the fact that not all elements were measured.

$Z=24$ and maximum around $Z=34$ persists for $n=7$ to $n=6$ transitions where nuclear absorption is not complete until $Z=70$. Therefore it appears that nuclear absorption from orbital states near the nuclear surface is not responsible for the unexpected behavior.

We can assume that practically all stopped kaons ultimately react with nucleons although this assumption should be checked by experiment. From bubble-chamber studies it has been observed that

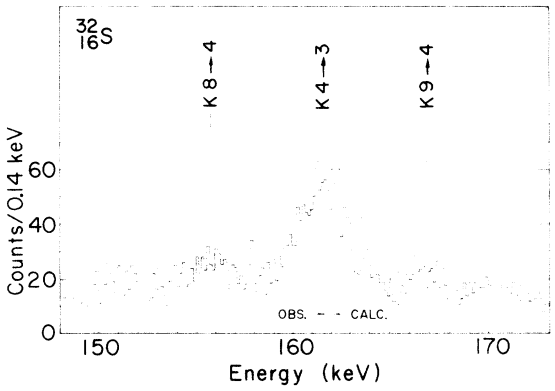

FIG. 11. Details of the kaonic x-ray spectrum of ^{32}S showing line broadening and energy shift of the $n=4\rightarrow3$ transition. These effects are due to the strong kaon-nucleon interaction. The dotted spectral line under the broadened $n=4\rightarrow3$ peak is the $n=6\rightarrow4$ line that actually appeared at 130 keV. The width of the $n=6\rightarrow4$ line represents the instrumental resolution and it was transplanted in order to illustrate the broadening of the $n=4\rightarrow3$ peak.

TABLE V. List of kaonic x-ray lines broadened and shifted in energy due to strong interaction effects. Energies are in keV. Calculated energies included corrections for first-order vacuum polarization; other corrections were negligible. Energies calculated by CERN were based on a kaonic mass of 493.73 MeV[a]; LBL used 493.84 MeV.[b]

A_Z	n_i	n_f	E_{calc}	E_{expt}	Width (keV)	Reference
^{10}B	3	2	43.576	43.368 ± 0.035	0.81 ± 0.10	CERN[a]
^{11}B	3	2	43.776	43.609 ± 0.035	0.70 ± 0.08	CERN[a]
^{12}C	3	2	63.317	62.73 ± 0.08	1.73 ± 0.15	CERN[a]
^{31}P	4	3	142.354	142.02 ± 0.08	1.44 ± 0.12	CERN[a]
S	4	3	162.141	161.57 ± 0.18	2.50 ± 0.32	LBL[c]
S	4	3	162.141	161.81 ± 0.15	2.23 ± 0.20	LBL[d]
S	4	3	162.107	161.56 ± 0.06	2.33 ± 0.06	CERN[a]
Cl	4	3	183.351	182.27 ± 0.22	2.79 ± 0.25	LBL[e]
Cl	4	3	183.306	182.54 ± 0.40	3.8 ± 1.0	CERN[a]

[a] Backenstoss *et al.*, Phys. Lett. B38, 181 (1972).
[b] *Review of Particle Properties* [Phys. Lett. B39, 1 (1972)].
[c] This experiment, detector 58A.
[d] This experiment, detector 148.
[e] This experiment, detector 239A.

0.026 ± 0.004 of the negative kaons stopped in ^{4}He decay at rest.[19] In other light elements, some of the kaons might decay during the deexcitation period of the atoms.

In our experiments we found that less than half the stopped kaons made x rays that we detected and that these x rays came from orbital transitions a few levels above the region of nuclear absorption. The intensities of lower-energy x rays were reduced below the limits of detectability by competition with Auger processes and by attenuation in the target material. All the x rays that we measured originated from hydrogenlike systems of mesonic orbits inside the atomic ground-state radius where, for kaons, $n < 31$.

To account for the vagary in intensities we can speculate that kaons were captured into angular momentum states with distributions that depended upon the electronic configurations of the atoms. Kaons in low angular momentum states have a high probability of nuclear absorption even though n is large. However, we do not know of a mechanism by which electronic configurations can influence angular momentum distributions in mesonic atoms. Perhaps the "sliding transitions" mentioned by Ruderman[20] have a bearing on the problem. These are transitions where l becomes smaller while n remains constant.

There are variations in the intensities of pionic x rays similar to those we have seen for kaons. Figure 12 was reproduced from the data of Table II from the thesis of Kunselman.[21] It shows the yields of $n = 4$ to $n = 3$ transitions in pionic atoms from $Z = 19$ to 53.

Our kaonic x-ray spectrum of ^{4}He is shown in Fig. 13. Previous attempts by Burleson, Cohen, Lamb, Michael, and Schluter and by Berezin, Burleson, Eartly, Roberts, and White[22] to measure ^{4}He x rays gave contradictory results. Although the first experiment by Burleson *et al.* claimed to have definitely observed a (6.7 ± 0.2)-keV line with apparently large absolute yield, the second experiment by Berezin *et al.* disclosed no identifiable x-ray lines from ^{4}He with yield limits of $K\alpha$ $(2p \rightarrow 1s) = 0.06 \pm 0.05$ and $L\alpha$ $(3d \rightarrow 2p) = 0.03 \pm 0.07$. Results of the present experiment are listed in Table IV. The sum of the intensities of the three observed lines shows that about 0.17 of the stopped kaons arrived at $n = 2$. Absence of x rays at 35 keV indicated that less than 0.004 kaons made transitions $n = 2 \rightarrow 1$. Additional com-

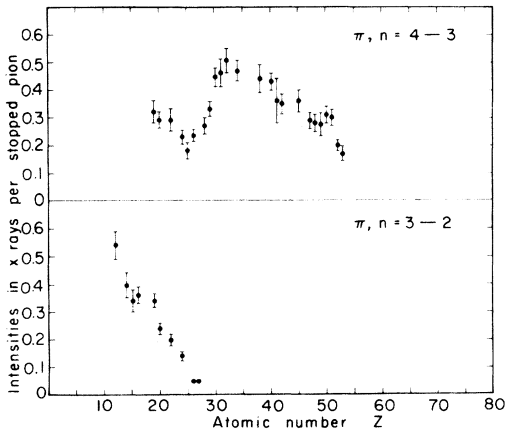

FIG. 12. Intensities vs Z of pion x-ray lines. Data were taken from the thesis of A. R. Kunselman, Lawrence Radiation Laboratory Report No. UCRL-18654, 1969.

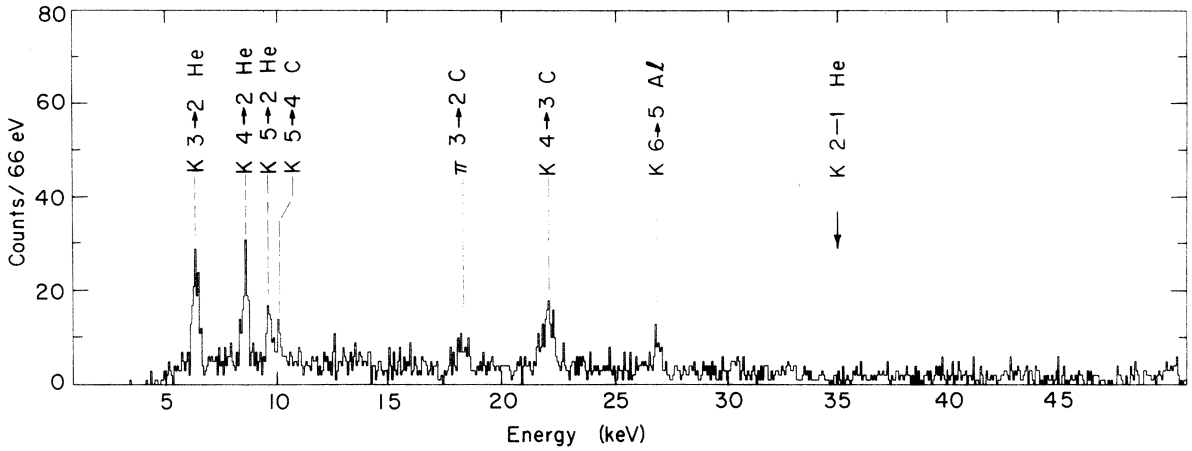

FIG. 13. Kaonic x-ray spectrum of ^{4}He with energy resolution 340 eV. Lines from C and Al came from particles stopped in the graphite energy degrader and the Al structure of the target.

ments on the ^{4}He experiments are contained in Ref. 11.

In the spectrum of ^{6}Li (see Fig. 14) we have several kaonic x-ray lines whose transitions end at $n=2$ and $n=3$. We found no energies that were different from those calculated by electromagnetic theory. The line due to Σ^- hyperonic transitions came at 11.50 keV as expected. We found no lines shifted in energy as suggested by Berezin *et al.*[23] At 18.4 keV there is a small peak from pions ($n=3\rightarrow 2$) landing in the C degrader. The pions most likely came from hyperon production and decay.

We noticed that in the spectrum of Li there were intervals around 6 keV where the background intensity was low. There was on hand a target of LiH, and realizing that the $n=2\rightarrow 1$ transition in kaonic hydrogen should be about 6.5 keV, we yielded to the temptation to make a run of kaons on LiH. There was no evidence for 6.5-keV x rays, but had capture on H and Li been proportional to Z, and had all the kaons captured by H made transitions to the ground state, we probably would have observed an effect.

In the course of investigating the intensities of kaonic x-ray lines of the isotopes of some elements, we made spectra of ^{167}Er and ^{170}Er. The nuclear characteristics of the two isotopes are quite different even though their constituents differ by only three neutrons. The nucleus $^{167}_{68}$Er has spin $\frac{7}{2}$, magnetic moment of -0.565 nuclear magnetons, and quadrupole moment of 2.83×10^{-24} cm^2.

Before nuclear absorption, the last transition in Er is $n=8\rightarrow 7$. Hyperfine splitting due to the nuclear magnetic moment is proportional to M_K^2 and is too small to observe for $n=7$. Splitting due to the electric quadrupole moment is proportional to M_K^3 and an effect is noticeable in the spectra of Fig. 15 where the $n=8\rightarrow 7$ line in ^{167}Er is "broadened" but the same line in ^{170}Er is sharp. We are indebted to Jenkins[24] for his calculation of the transition energies and relative intensities. According to selection rules there are eight components of the ^{167}Er line that have significant intensities out of a total of 21 possibilities. Our spectrometer could not resolve individual components, therefore the ensemble appears as a group of peaks, but the peaks are mostly statistical fluctuations. The maximum difference in energy between intense components is 4.4 keV and this is compatible with the observed "broadening."

In the spectrum of ^{55}Mn (see Fig. 16) we note an unusual line at 126 keV. It has about the same intensity as the principal transition $n=6\rightarrow 5$, but its energy corresponds to the kaonic transition $n=9\rightarrow 6$. In all other elements the $\Delta n=-3$ transitions have an intensity about 0.05 that of the principal lines. When we realized that the first excited state of the ^{55}Mn nucleus was 126 keV, we naturally conjectured that some kind of coupling between the atomic and nuclear states caused an

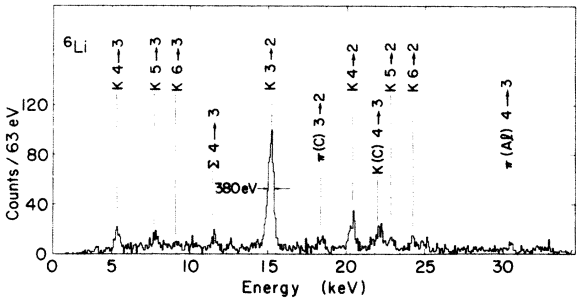

FIG. 14. Kaonic x-ray spectrum of ^{6}Li. Within experimental errors, all the lines have energies that agree with electromagnetic theory.

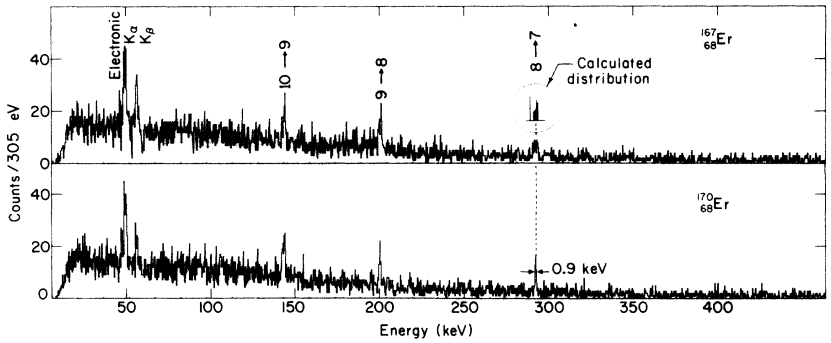

FIG. 15. Kaonic x-ray spectra of $^{167}_{68}$Er and $^{170}_{68}$Er showing the effect of the large electric quadrupole moment on the $n=8\rightarrow 7$ transition in ^{167}Er. In ^{170}Er the $n=8\rightarrow 7$ line is sharp, in ^{167}Er it is split into unresolved components and thereby appears to be broadened.

enhancement of the line.[25] However, there are serious drawbacks to this idea: the parity of the nuclear ground state and the excited state are the same whereas electric dipole radiation of an atom requires a change in parity. More serious is the difference in lifetimes of the states: τ of the nuclear level is 3×10^{-10} sec while lifetimes for radiation of the kaonic states are about 10^{-15} sec. If we imagine that the energy of the atomic state were somehow transferred to the nucleus and raised it to its excited level, the kaon would reach the nucleus and disrupt it before the nucleus could radiate. But, it appears improbable that target nuclei could be so intensely excited by direct interactions between stopping kaons or their products. We found no indication of radiation from the first excited state of $^{127}_{53}$I at 58 keV. (Neither is there a kaonic transition of the same energy.) But an early paper of Temmer and Heydenburg[26] indicates that ^{55}Mn was more easily excited by α particles than were other nuclei that they studied. The matter of the anomalously intense line in kaonic ^{55}Mn is in abeyance until the next experiment.

B. Σ^--hyperonic atoms

A kaonic atom ceases to exist when the orbiting kaon reaches the nucleus and is absorbed by one of the processes listed in Table VI. We note that about 8% of kaons stopped in nuclear emulsion resulted in the ejection of Σ^- hyperons[27] and about 14% made Σ^- in CF_3Br (heavy-liquid bubble chamber).[28] The average energy of the hyperons was about 20 MeV. In our experiment most of the hyperons that emerged from target nuclei remained within the targets and either decayed in flight or were captured into Σ^- hyperonic atoms. X-ray intensities of the observed principal transitions amounted to about 0.015 per stopped kaon.

Interest in Σ^- hyperonic atoms stems mainly from the idea that it may be possible to determine the magnetic moment of Σ^- hyperons by studies of their atomic x-ray lines. The magnetic moment of Σ^- has not yet been measured. SU(3) theory predicts that its value is the negative difference between the proton and neutron magnetic moments: $\mu_{\Sigma^-}=-(\mu_p-\mu_n)=-0.88\Sigma$ magnetons. According to quark-model theory, $\mu_{\Sigma^-}=-\frac{1}{3}\mu_p=-0.93\Sigma$ magnetons.[29]

Owing to the spin and magnetic moment, the energy levels are doublets. For orbiting particles with no anomalous magnetic moment, the splitting for circular orbits would amount to

$$\Delta E=\tfrac{1}{2}Mc^2\frac{\alpha^4Z^4}{(n-1)n^4},$$

where M is the reduced mass of the system and α is the fine-structure constant. But according

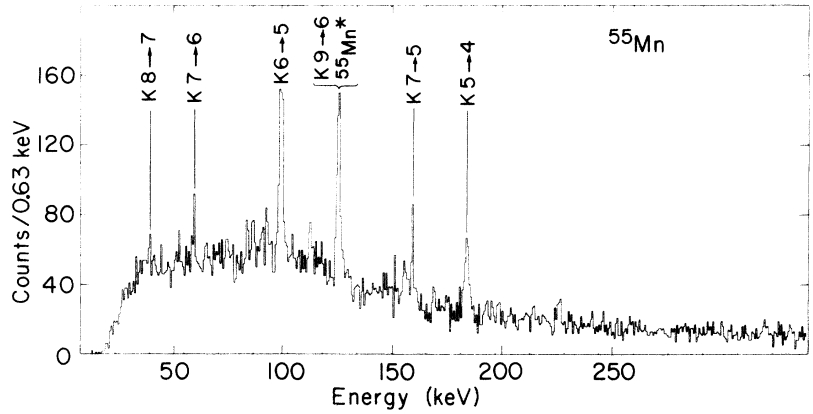

FIG. 16. Kaonic x-ray spectrum of $^{55}_{25}$Mn.

TABLE VI. Hyperon production.

Reaction	Relative occurrences: Nuclear emulsion[a]	CF_3Br[b]
$K^- + p \rightarrow \Sigma^- + \pi^+$	0.030 ± 0.007	0.111 ± 0.005
$\rightarrow \Sigma^+ + \pi^-$	0.067 ± 0.008	0.113 ± 0.014
$\rightarrow \Sigma^0 + \pi^0$	•••	0.096 ± 0.015[c]
$K^- + n \rightarrow \Sigma^- + \pi^0$	0.053 ± 0.011[d]	0.032 ± 0.005[c]
$\rightarrow \Sigma^0 + \pi^-$	0.031 ± 0.01	0.032 ± 0.005
$K^- + p \rightarrow \Lambda + \pi^0$	•••	0.118 ± 0.012[c]
$K^- + n \rightarrow \Lambda + \pi^-$	0.128 ± 0.019	0.236 ± 0.024
$K^- + 2N$ (nonpionic) account for about 0.2		

[a] Reference 27.
[b] Reference 28.
[c] Calculated.
[d] No visible π^+ or π^-.

to Bethe and Salpeter[30] the anomalous part of the magnetic moment contributes twice as much to the splitting as does the ordinary moment (Bethe and Salpeter were considering the hydrogen atom where $g_1 \ll 1$, but g_1 is not restricted. For example, in antiprotonic atoms the level splitting is expected to be $E = \frac{1}{2} M_p c^2 \alpha^4 Z^4/(n-1)n^4 \times [1 + 2(2.79 - 1)]$.):

$$\Delta E = \tfrac{1}{2} Mc^2 \frac{\alpha^4 Z^4}{(n-1)n^4} (1 + 2g_1),$$

where g_1 is the anomalous part of the magnetic moment:

$$\mu = \frac{eh}{2Mc} (1 + g_1).$$

If $\mu_{\Sigma^-} = -0.9\Sigma$ magnetons, $g_1 = -0.1$ and

$$\Delta E = \tfrac{1}{2} Mc^2 \frac{\alpha^4 Z^4}{(n-1)n^4} (1 - 0.2).$$

For example, consider transitions between circular orbits $n = 6 \rightarrow 5$. Only transitions of $\Delta j = -1$ have significant (and almost equal) intensities; therefore the x-ray line is a doublet and the splitting is $\Delta E(n=5) - \Delta E(n=6)$. In the Cl spectrum of Fig. 6 the splitting would amount to 27 eV for $\mu_{\Sigma^-} = -0.9$. Of course, this is far from the resolution capability of present techniques.

Since the level splitting of circular orbits is proportional to Z^4/n^5, we would expect that the doublets would be easier to observe in heavy elements. According to Zieminska[31] the probability that stopped negative kaons result in the formation of Σ^- hyperonic atoms in Pb is about half the probability of formation in light elements.

The first x rays from Σ^- hyperonic atoms appeared in a kaonic spectrum of $^{39}_{19}K$ taken by Wiegand.[4] Since then many Σ^- x-ray lines have been seen in spectra taken at CERN[32] and LBL. Table VII presents a list of Σ^- hyperonic x rays observed in the present experiment.

Fox *et al.*[33] have recently reported limits on the Σ^- magnetic moment through observation of the x-ray line of Σ^- transitions from $n = 12$ to $n = 11$ in Pb. For $\mu = -1$ sigma magneton, the splitting is expected to be 0.187 keV. Their detector resolution was 1.3-keV FWHM and therefore could not produce convincing results from the relatively

TABLE VII. Intensities of Σ^- hyperonic x-ray lines observed in the present experiment. Calculated energies do not include vacuum polarization or corrections for finite nuclear size. Intensities are in x rays per stopped *kaon*.

Target A_Z	Transition n_i	n_f	Calculated transition energy (keV)	I x rays per K_{stop}	$\pm \Delta I/I$ Use for error in relative I	$\pm \Delta I$ Use for error in absolute I
^{6}Li	4	3	11.5	0.011	0.25	0.004
^{7}Li	4	3	11.9	0.009	0.24	0.003
^{12}C	4	3	50.4	0.012	0.39	0.006
$H_2{}^{16}O$	5	4	42.5	0.005	0.40	0.002
S	7[a]	6	57.9	0.021	0.10	0.004
	6	5	96.0	0.011	0.11	0.002
CCl_4	8	7	42.5	0.008	0.50	0.004
	7[a]	6	65.5	0.023	0.11	0.004
	6[b]	5	108.7	0.021	0.07	0.004
Fe	7[a]	6	155.4	0.023	0.52	0.013
^{59}Co	7[a]	6	167.8	0.022	0.42	0.010
Ge	9	8	105.3	0.040	0.28	0.013
	8	7	153.6	0.037	0.23	0.011
Se	8	7	173.6	0.042	0.21	0.011

[a] Includes K, $n = 10 \rightarrow 6$ which is estimated to contribute about 0.01 x rays per stopped kaon.
[b] Possibly includes a contribution from $^{19}F^*$ nuclear γ rays.

weak line. In nuclear magneton units, the value reported is $-1.6 < \mu < 0.8$ and is based on a fit that corresponds to a χ^2 of 50 for 34 degrees of freedom (confidence level $\simeq 0.04$).

Hyperons are absorbed near the surfaces of nuclei in a manner analogous to kaon absorption, except that Σ^- reacts only with protons: $\Sigma^- + p \rightarrow \Lambda + n$. Σ^- has no known resonance to complicate its behavior as in the case of K^- mesons. Therefore, it might become a sensitive probe of the proton distribution in the extremely rarified "nuclear atmosphere."

C. Pionic x rays

A few x rays emitted by pionic atoms were found in the kaonic spectra. We believe that the pions came from kaonic reactions on nucleons and the subsequent decay of the hyperons, but not from pions in the beam. The pionic lines came from target atoms except for the ^{4}He and Li spectra where they came from the aluminum target structure and the carbon degrader.

D. Nuclear γ rays

Some specific γ rays following kaon capture by ^{208}Pb and ^{17}O were predicted by Bloom, Weiss, and Shakin.[34] Probably because of insufficient experimental effort, these particular γ rays have not been seen. Several studies have been made of nuclear γ rays resulting from stopped muons and pions.[35] Recently nuclear γ rays from stopped kaons have begun to emerge.[36] A few were seen in the spectra of S and Cl in the present experiment as indicated in Fig. 6. The paucity of γ rays could be attributed to their low intensity and the general trend of their energies to be higher than

TABLE VIII. Nuclear γ rays due to stopped kaons. Column 1 gives the excited nuclei whose energy levels corresponded to the observed γ rays. In column 2 are listed energies of the excited states found in Ref. 16 and Nuclear Data Sheets. Column 3 gives the targets from which the γ rays were emitted. Column 4 lists the intensities in γ rays per stopped *kaon*. Estimated errors are given in columns 5 and 6.

Excited nucleus	γ-ray energy (keV)	Target	I γ rays per K_{stop}	$\Delta I/I$ Use for error in relative I	ΔI Use for error in absolute I
^{19}F	109.9	S	0.007	0.17	0.002
		CCL_4	0.021	0.07	0.004
		$Na^{35}Cl$	0.021	0.16	0.004
		$Na^{37}Cl$	0.024	0.16	0.005
	197.2	S	0.010	0.22	0.003
^{32}P	78.1	S	0.006	0.20	0.001
		CCl_4	0.025	0.08	0.004
		$Na^{35}Cl$	0.025	0.25	0.007
		$Na^{37}Cl$	0.017	0.35	0.006
^{47}Ti	158.8	^{51}V	0.024	0.33	0.009
		Cr	0.050	0.17	0.011
		Fe	0.033	0.30	0.011
		^{59}Co	0.015	0.46	0.008
		^{58}Ni[a]	0.014	0.50	0.007
		^{62}Ni[a]	0.021	0.50	0.011
		^{65}Cu	0.035	0.21	0.009
		Zn	0.017	0.30	0.006
^{49}V	152.9	Cr	0.023	0.41	0.010
^{50}V	226.2	Cr	0.056	0.25	0.017
		^{55}Mn	0.029	0.35	0.011
^{55}Mn	125.9	^{55}Mn	0.100	0.08	0.02
		Fe	0.027	0.24	0.008
		^{59}Co	0.019	0.37	0.008
^{57}Fe	122.0	^{59}Co	0.021	0.44	0.010
		^{62}Ni	0.025	0.24	0.007
		Zn[b]	0.011	0.50	0.006
^{61}Ni	67.4	^{63}Cu	0.052	0.44	0.024
		^{65}Cu	0.039	0.59	0.024
^{42}K	107.1	Zn	0.019	0.70	0.014

[a] Estimated background from K $9 \rightarrow 6$ was subtracted.
[b] Estimated background from K $10 \rightarrow 7$ was subtracted.

mesonic x-ray energies and thus to be missed by x-ray spectrometers. Table VIII lists the nuclear γ rays observed in the present experiment.

Interest in kaon-induced nuclear γ rays is concerned with the formation of the excited nuclei. High-resolution semiconductor detectors give the energies of the lines with accuracy sufficient to identify unambiguously the excited nuclear states that emit them. For example, we observed a (78.1 ± 0.1)-keV line in the kaonic spectra of NaCl, CCl_4, and S. According to nuclear-data tabulations, the first excited state of ^{32}P emits γ rays of precisely the same energy. Therefore, we know that $^{32}P^*$ nuclei existed in connection with stopped kaons. In the spectrum of ^{32}S we identified nuclear γ-ray lines from the two lowest excited states of ^{19}F. Because strangeness must be conserved, it is reasonable to postulate that hypernuclei were also involved in the reactions. Yet we cannot be sure that all the γ rays came from nuclei of the atoms in which the kaons were captured. In Ref. 36 we speculated on the possible formation of hypernuclei and the emission of γ rays through the reactions:

$$K^- + {}^{32}_{16}\mathrm{S} \rightarrow {}^{32}_{\Lambda}\mathrm{P} + \pi^0 \searrow {}^{32}_{15}\mathrm{P}^* + \pi^0,$$

$$K^- + {}^{32}_{16}\mathrm{S} \rightarrow {}^{19}_{9}\mathrm{F}^* + {}^{13}_{\Lambda}\mathrm{C} \rightarrow {}^{19}_{9}\mathrm{F}^* + 2\,{}^4\mathrm{He} + n + {}^{4}_{\Lambda}\mathrm{He}.$$

In a recent experiment Barnes *et al.*[6] identified about 20 nuclear γ rays in association with kaons stopped in targets of natural isotopic mixtures of Cu and Ni. They speculated that the nuclear γ-ray spectra following K^- capture in Ni and Cu show a pattern that implied the removal of one, two, or three α particles.

Except for the special case of ^{55}Mn, which was discussed earlier, all the nuclear γ rays reported have lower intensities than the principal kaonic x-ray lines. Intensities of the lines observed in our experiment ranged from about 0.01 to 0.1 γ-ray per stopped kaon.

VII. CONCLUDING REMARKS

Considerable progress has been made in the experimental studies of kaonic and hyperonic atoms. Kaonic x-ray spectra of the elements have been investigated and the intensities of the principal low-n transitions measured. Some spectra have been taken in detail sufficient to show line broadening and energy shift owing to strong interaction effects. But the interpretation of the results has become entangled in complications that were not expected when predictions were made on the usefulness of kaons as probes of the distribution of nuclear matter. The cutoffs of small n transitions as Z increases are accepted as being due to kaons encountering nuclear matter when they are mostly in orbits of maximum angular momenta. However, the simple interpretation that the capture rate be given by

$$R_{\mathrm{capt}} \approx W \int \rho(r) |\Psi_K(r)|^2 d^3r$$

had to be abandoned. In the above equation W is proportional to the K^--nucleon reaction rate, $\rho(r)$ is the nuclear density, and $\Psi_K(r)$ the unperturbed kaon wave function of the orbit from which capture occurs.

Several effects enter to upset the simple picture of kaon capture at the periphery of nuclei where the nuclear density is admittedly low. Among them are (i) the absorption is so strong that the kaonic wave function is distorted,[37] (ii) the broad resonance, $Y_0^*(1405)$, lies at -27 MeV in the K^--p system and enhances the capture of kaons by protons,[38] and (iii) the finite interaction range of the particle involved should be taken into account. As a reference to these remarks, we suggest the comments of Alberg, Henley, and Wilets.[39] For a discussion of mesonic capture processes, see the recent review article by Ponomarev.[40]

VIII. ACKNOWLEDGMENTS

Jeff Gallup contributed greatly to the experiment, especially by his calibration of the detectors and his expert use of the LBL Computer Center.

It is a pleasure to express our appreciation to members of the LBL Nuclear Instrumentation Group, Fred Goulding, Richard Pehl, William Hansen, Don Landis, Dick Cordi, and Don Malone. They furnished the semiconductor detectors and associated electronic apparatus. The data-handling system to put information on magnetic tape was produced by Fred Kirsten, Bob Rudden, and Mike Wolverton.

We thank Donald Brandshaft, A. R. Kunselman, and Gary Lum for helping in early stages of the experiment.

Walter Hartsough and his Bevatron operations crew did their usual splendid job in sending about 10^{17} protons through our kaon-production target.

*Work done under the auspices of the United States Atomic Energy Commission.

[1]M. Camac, A. D. McGuire, J. B. Platt, and H. J. Schulte, Phys. Rev. 88, 134 (1952).
[2]Val. L. Fitch and James Rainwater, Phys. Rev. 92, 789 (1953).
[3]Clyde E. Wiegand and Dick A. Mack, Phys. Rev. Lett. 18, 685 (1967).
[4]Clyde E. Wiegand, Phys. Rev. Lett. 22, 1235 (1969).
[5]G. Backenstoss, A. Bamberger, J. Egger, W. D. Hamilton, H. Koch, U. Lynen, H. G. Ritter, and H. Schmitt, Phys. Lett. B 32, 399 (1970).
[6]P. D. Barnes, R. A. Eisenstein, W. C. Lam, J. Miller, R. B. Sutton, M. Eckhause, J. Kane, R. E. Welsh, D. A. Jenkins, R. J. Powers, R. Kunselman, R. P. Redwine, R. E. Segel, and J. P. Schiffer, Phys. Rev. Lett. 29, 230 (1972).
[7]C. S. Wu and Lawrence Wilets, Ann. Rev. Nucl. Sci. 19, 527 (1969).
[8]G. Backenstoss, Ann. Rev. Nucl. Sci. 20, 467 (1970).
[9]P. B. Jones, Philos. Mag. 3, 33 (1958); D. H. Wilkinson, in *Proceedings of the Rutherford Jubilee International Conference, Manchester, 1961*, edited by J. B. Birks (Heywood and Company, London, 1962), p. 339.
[10]E. H. S. Burhop, Ed., *High-Energy Physics, Vol. III*, (Academic, New York–London, 1969), p. 109; Y. N. Kim, *Mesonic Atoms and Nuclear Structure* (North-Holland, Amsterdam, 1971).
[11]Clyde E. Wiegand and Richard H. Pehl, Phys. Rev. Lett. 27, 1410 (1971).
[12]W. L. Hansen, Nucl. Instrum. Methods 94, 377 (1971); D. A. Landis, F. S. Goulding, and J. M. Jaklevic, Nucl. Instrum. Methods 87, 211 (1970).
[13]Richard H. Pehl and Fred S. Goulding, Nucl. Instrum. Methods 81, 329 (1970).
[14]Richard H. Pehl, Richard C. Cordi, and Fred S. Goulding, IEEE Trans. Nucl. Sci. 19, 265 (1972).
[15]W. H. McMaster, N. Kerr Del Grande, J. H. Mallett, and J. H. Hubbell, Lawrence Radiation Laboratory Report No. UCRL-50174, 1969 (unpublished).
[16]C. M. Lederer, J. M. Hollander, and I. Perlman, *Table of Isotopes* (Wiley, New York, 1967).
[17]E. Fermi and E. Teller, Phys. Rev. 72, 399 (1947).
[18]G. Backenstoss, A. Bamberger, I. Bergstrom, P. Bounin, T. Bunaciu, J. Egger, S. Hultberg, H. Koch, M. Krell, U. Lynen, H. G. Ritter, A. Schwitter, and R. Stearns, Phys. Lett. B 38, 181 (1972).
[19]K. Bunnell, M. Derrick, T. Fields, L. G. Hyman, G. Keyes, J. G. Fetkovich, J. McKenzie, and I-T. Wang, *Proceedings of International Conference on Hypernuclear Physics* (Argonne National Laboratory, Argonne, Ill., 1969), p. 753.
[20]M. Ruderman, Phys. Rev. 118, 1632 (1960).
[21]A. R. Kunselman, Lawrence Radiation Laboratory Report No. UCRL-18654, 1969 (unpublished).
[22]G. R. Burleson, D. Cohen, R. C. Lamb, D. N. Michael, and R. A. Schluter, Phys. Rev. Lett. 15, 70 (1965); D. N. Michael, Phys. Rev. 158, 1343 (1967); S. Berezin, G. Burleson, D. Eartly, A. Roberts, and T. O. White, Phys. Lett. B 30, 27 (1969).
[23]S. Berezin, G. Burleson, D. Eartly, A. Roberts, and T. O. White, Nucl. Phys. B 16, 389 (1970).
[24]D. A. Jenkins (private communication).
[25]Gary L. Godfrey and Clyde E. Wiegand, Lawrence Berkeley Laboratory Report No. LBL-776, 1972 (unpublished).
[26]G. M. Temmer and N. P. Heydenburg, Phys. Rev. 93, 351 (1954).
[27]B. Bhowmik *et al.*, Nuovo Cimento 14, 315 (1959). (1959).
[28]G. Schorochoff, Universite Libre de Bruxelles, Institut de Physique, Bulletin No. 40, 1969.
[29]J. J. J. Kokkedee, *The Quark Model* (Benjamin, New York–Amsterdam, 1969), p. 187.
[30]H. A. Bethe and E. E. Salpeter, *Quantum Mechanics of One- and Two-Electron Atoms* (Academic, New York, 1957), p. 58.
[31]D. Zieminska, Phys. Lett. B 37, 403 (1971).
[32]G. Backenstoss, T. Bunaciu, S. Charalambus, J. Egger, H. Koch, A. Bamberger, U. Lynen, H. G. Ritter, and H. Schmitt, Phys. Lett. B 33, 230 (1970).
[33]J. D. Fox, W. C. Lam, P. D. Barnes, R. A. Eisenstein, J. Miller, R. B. Sutton, D. A. Jenkins, M. Eckhause, J. R. Kane, B. L. Roberts, R. E. Welsh, and A. R. Kunselman, Phys. Rev. Lett. 31, 1084 (1973).
[34]S. D. Bloom, M. S. Weiss, and M. Shakin, Phys. Rev. C 5, 238 (1972).
[35]See, e.g., G. Backenstoss, S. Charalambus, H. Daniel, W. D. Hamilton, U. Lynen, Ch. von der Malsburg, G. Poelz, and H. P. Povel, Nucl. Phys. A 162, 541 (1971); W. J. Kossler, H. O. Funsten, B. A. MacDonald, and W. F. Lankford, Phys. Rev. C 4, 1551 (1971).
[36]Clyde E. Wiegand, Jeffrey M. Gallup, and Gary L. Godfrey, Phys. Rev. Lett. 28, 621 (1972).
[37]T. E. O. Ericson and F. Scheck, Nucl. Phys. B 19, 450 (1970); Max Krell, Phys. Rev. Lett. 26, 584 (1971); Ryoichi Seki, Phys. Rev. Lett. 29, 240 (1972).
[38]S. D. Bloom, M. H. Johnson, and E. Teller, Phys. Rev. Lett. 23, 28 (1969); William A. Bardeen and E. Wayne Torigoe, Phys. Lett. B 38, 135 (1972).
[39]M. Alberg, E. M. Henley, and L. Wilets, Comments Nucl. Part. Phys. 5, 1 (1972).
[40]L. I. Ponomarev, Ann. Rev. Nucl. Sci. 23, 395 (1973).